# Fano interferences in environment-enabled electron capture

Axel Molle,[1] Alain Dubois,[1] Jimena D. Gorfinkiel,[2] Lorenz S. Cederbaum,[3] and Nicolas Sisourat[1,*]

[1]*Sorbonne Université, CNRS, Laboratoire de Chimie Physique - Matière et Rayonnement, F-75005 Paris, France*

[2]*School of Physical Sciences, The Open University, Walton Hall, Milton Keynes MK7 6AA, United Kingdom*

[3]*Theoretische Chemie, Physikalisch-Chemisches Institut, Universität Heidelberg, Im Neuenheimer Feld 229, Heidelberg D-69120, Germany*

(Received 28 October 2020; accepted 4 January 2021; published 19 January 2021)

Interatomic Coulombic electron capture (ICEC) is an environment-assisted process in which a free electron can efficiently attach to a quantum system by transferring the excess energy of the electron capture to a neighbor ionizing it. Using the *ab initio R*-matrix method, we show that Fano profiles, resulting from interferences between the ICEC final states and resonant states, appear in the ICEC cross sections even at extremely large system-neighbor separations. We identify several types of resonant states depending on their decay pathways which may involve long-range electron and energy transfer. ICEC is a fundamental process and the interferences lead to substantial enhancement or decrease of the cross sections. The present investigation is therefore of general relevance in many contexts wherever electron capture in an environment takes place.

DOI: 10.1103/PhysRevA.103.012808

## I. INTRODUCTION

Fano profiles [1] are universal line shapes which are observed in many contexts in physics, such as photoionization [2,3] and photoabsorption [4,5] spectroscopies, electron-molecule (see, e.g., [6,7]), microwave [8], and Raman [9,10] scattering, scanning microscopy tunneling [11–13], transport in single-electron transistors [14], interferometers [15–17], and carbon nanotubes [18,19], as well as in plasmonic nanostructures and metamaterials [20]. Generally speaking, these profiles are signatures of interference between a quasibound (resonant) state and a continuum. Fano [1] was the first to derive the underlying theory for the study of the autoionization of the helium atom after inelastic electron scattering.

Interatomic Coulombic electron capture (ICEC) is a unique inelastic electron scattering process, which can only take place in an environment, i.e., when the system capturing the electron possesses at least one neighbor [21,22]. In the ICEC mechanism, a free electron can efficiently attach to an atomic, molecular, or quantum dot system (see [23–25] and references therein for studies of ICEC in quantum nanomaterials) by transferring the excess energy to a neighbor, which is then ionized (see Fig. 1). A strong enhancement of the electron attachment (or capture) cross sections in several systems due to the ICEC process has been demonstrated using an analytical formula which is valid at large distances between the system and neighboring species [21,22]. Using the *ab initio R*-matrix method, it was recently shown that the ICEC cross sections may even be several orders of magnitude higher than predicted by the analytical formula and dominate, by far, other competing processes [26].

In this work, we demonstrate that Fano profiles appear in the ICEC cross sections, even at extremely large system-neighbor separations. These profiles result from the interferences between the ICEC final states and resonant states in which the incoming free electron temporarily binds to the system or to the neighboring species. The proton-water setup is used here as a model to illustrate this phenomenon and its richness. Several types of resonant states are identified and their mechanism to release an electron and contribute to the overall ICEC cross section is discussed and found to bear some surprises. From the investigation and analysis, it is clear that the presence of Fano profiles in the ICEC cross sections is general. The sheer presence of the interferences involving the environment and causing substantial enhancement or decrease of the cross sections, even at large distances between the system and its environment, is of basic interest and of relevance in many contexts wherever electron capture plays a role.

## II. METHODS AND COMPUTATIONAL DETAILS

The cross sections of ICEC in the proton-water setup were computed with the *R*-matrix method as implemented in the UKRmol+ package. A review of the *R*-matrix method can be found in [27] and details of the UKRmol+ package are presented in [28]. In the following, we summarize the method and the implementation used in this work. In the *R*-matrix approach, the configuration space is partitioned into an inner and an outer region defined by a sphere of radius $a$ around the center of mass of the full system. The inner region contains the multielectron description of the full system composed of $N+1$ electrons (i.e., 11 electrons in this work). In the outer region only, a single free electron is treated and its interaction with the $N$ remaining electrons (i.e., 10 electrons) is described in terms of a multipole expansion. The $R$ matrix links the two regions. The ICEC cross sections are obtained after the analysis of the wave function in the outer region.

In our calculations, we assumed a symmetric planar geometry where the oxygen atom points to the proton and the

*nicolas.sisourat@upmc.fr

 

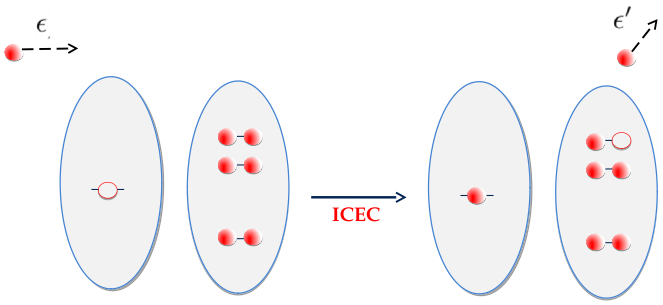


FIG. 1. ICEC scheme: A free electron attaches to the species on the left. The attachment energy is transferred to the one on the right, which is then ionized.

water is in its isolated ground-state equilibrium geometry. The calculations are performed in the $C_{2v}$ point group and within the fixed-nuclei approximation. We used state-averaged complete active space self-consistent field (CASSCF) orbitals optimized for the three lowest singlet $A_1$ states: $H^+$ - $H_2O(\tilde{X})$, $H^+$ - $H_2O(\tilde{B})$, and $H(1s) - H_2O^+(3a_1^{-1})$. The active space includes the following orbitals: $1s_O$, $2s_O$, $1s_H$, $3a_1$, $4a_1$, $1b_1$, $1b_2$, and $2b_2$. In the close-coupling expansion, 18 target states (3 singlet and 3 triplet in each $A_1$, $B_1$, and $B_2$ symmetry), obtained from a full configuration interaction (CI) in the CAS active space, were included. They correspond to the 11 lowest states of $H^+$ - $H_2O$ and 7 lowest states of $H(1s) - H_2O^+$. The latter are the final states of the ICEC processes. The computed energies of the target states are given in Table I for a distance $R$ between the proton and the oxygen atom of 8 Å.

The cc-pVDZ basis set was used and the CASSCF orbitals were optimized using the MOLPRO package [29,30]. We employed "continuum" orbitals with angular momentum up to $\ell = 6$, which are described with 25 B-spline-type orbitals of order 6 in each $\ell$. The $R$-matrix radius $a$ was fixed at 25 a.u. and the maximum values in the Legendre expansion of the mixed nuclear attraction and two-electron integrals (see [28] for further details on the implementation and parameters) were fixed at 35 and 45, respectively. Convergence with respect to the numerical parameters was checked by performing additional calculations with (i) the $R$-matrix radius fixed at 30 and 35 a.u. and (ii) the maximum values in the Legendre expansion of the mixed nuclear attraction and two-electron integrals fixed at 40 and 50, respectively. For the outer-region calculations, the $R$ matrix is propagated from $a$ to 80 a.u. The maximum multipole retained in the expansion of the long-range potential was set to 2.

TABLE I. Computed relative energies (in eV) of the target states included in the $R$-matrix calculations for $R = 8$ Å. The absolute ground-state energy is −76.1274 a.u. The initial ICEC state [$H^+$-$H_2O(X)$] is underlined, the final ICEC states [$H(1s) - H_2O^+$] are in black, and the lowest excited electronic states involving neutral water ($H^+$-$H_2O^*$) are in bold.

| Spin | Sym. | $E$ (eV) | State |
|---|---|---|---|
| Singlet | $B_1$ | 0.0 | $H(1s)$-$H_2O^+(1b_1^{-1})$ |
| Triplet | $B_1$ | 0.0 | $H(1s)$-$H_2O^+(1b_1^{-1})$ |
| Singlet | $A_1$ | 2.29 | $H(1s)$-$H_2O^+(3a_1^{-1})$ |
| Triplet | $A_1$ | 2.29 | $H(1s)$-$H_2O^+(3a_1^{-1})$ |
| <u>Singlet</u> | <u>$A_1$</u> | <u>2.50</u> | <u>$H^+$-$H_2O(\tilde{X})$</u> |
| Singlet | $B_2$ | 6.66 | $H(1s)$-$H_2O^+(1b_2^{-1})$ |
| Triplet | $B_2$ | 6.66 | $H(1s)$-$H_2O^+(1b_2^{-1})$ |
| **Triplet** | $\boldsymbol{B_1}$ | **9.29** | **$H^+$-$H_2O^*(^3B_1)$** |
| **Singlet** | $\boldsymbol{B_1}$ | **9.95** | **$H^+$-$H_2O^*(^1B_1)$** |
| **Triplet** | $\boldsymbol{A_1}$ | **11.93** | **$H^+$-$H_2O^*(^3A_1)$** |
| **Singlet** | $\boldsymbol{A_1}$ | **12.85** | **$H^+$-$H_2O^*(^1A_1)$** |
| Triplet | $B_1$ | 14.70 | $H(1s)$-$H_2O^+(^4B_1)$ |
| **Triplet** | $\boldsymbol{B_2}$ | **15.49** | **$H^+$-$H_2O^*(^3B_2)$** |
| **Triplet** | $\boldsymbol{B_1}$ | **15.74** | **$H^+$-$H_2O^*(^3B_1)$** |
| **Singlet** | $\boldsymbol{B_1}$ | **15.74** | **$H^+$-$H_2O^*(^1B_1)$** |
| **Singlet** | $\boldsymbol{A_1}$ | **15.87** | **$H^+$-$H_2O^*(^1A_1)$** |
| **Triplet** | $\boldsymbol{A_1}$ | **15.87** | **$H^+$-$H_2O^*(^3A_1)$** |
| **Singlet** | $\boldsymbol{B_2}$ | **16.69** | **$H^+$-$H_2O^*(^1B_2)$** |

## III. RESULTS AND DISCUSSION

In Table I, the initial ICEC state [$H^+$-$H_2O(\tilde{X})$] is underlined, the final ICEC states [$H(1s) - H_2O^+$] are in black, and the lowest excited electronic states of water in the presence of the proton ($H^+$-$H_2O^*$) are in bold. In our calculations, ICEC leading to the lowest $B_1$ and $A_1$ states of the water cation is allowed for any incoming electron energies, while the ICEC channels to the lowest $B_2$ states open at electron energy above 4.16 eV. Note that the computed relative energies, reported in Table I, are in good agreement with the energy difference between the states of the water cation [31] and the excitation thresholds of water [32]. The presence of the proton at the large distance of $R = 8$ Å is expected to only marginally affect these quantities.

In the limit of large $R$, the ICEC cross sections can be obtained from the photoionization cross sections of atomic hydrogen and isolated water ($\sigma_{\rm PI}^{(H)}$ and $\sigma_{\rm PI}^{(H_2O)}$) according to [21,22] (so-called virtual photon approximation)

$$\sigma_{\rm ICEC}(\epsilon) = \frac{3\hbar^4 c^2}{8\pi m_e}\frac{g_H}{g_{H^+}}\frac{\sigma_{\rm PI}^{(H)}(\epsilon)\sigma_{\rm PI}^{(H_2O)}(\epsilon')}{\epsilon R^6 E_{vph}^2}, \qquad (1)$$

where $\epsilon$ and $\epsilon'$ are the energies of the incoming and outgoing electrons, respectively, i.e., of the electron impinging on $H^+$ and of the electron emitted from $H_2O$ (see Fig. 1). The statistical weights of the quantum states are $g_H = 2$ and $g_{H^+} = 1$. The energy transferred between the species is $E_{vph} = {\rm IP}_H + \epsilon$, where ${\rm IP}_H = 13.61$ eV is the ionization potential of atomic hydrogen. In the following, we consider only ICEC processes for which the electron is captured in the ground state of hydrogen. The photoionization cross sections were taken from [33–35].

To compare, on the same scale, the ICEC cross sections computed at different $R$, we multiplied them by $R^6$. The results are reported in Fig. 2, where the cross sections from Eq. (1) are compared to those from the $R$-matrix calculations. To illustrate the Fano profiles in the ICEC cross sections, we consider in this work only large $R$ for which the virtual photon approximation is valid ($R \geqslant 6$ Å). However, we have also computed the *ab initio* ICEC cross sections for shorter $R$: these cross sections (not shown) are much larger than predicted by Eq. (1), as observed in our previous work [26]. Such enhancement comes from the contributions of the orbital overlaps

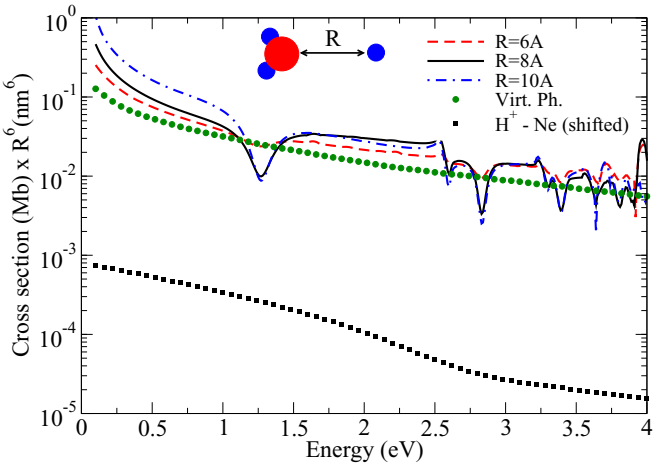


FIG. 2. Total ICEC cross sections [for $e + \mathrm{H}^+\text{-}\mathrm{H_2O}(\tilde{X}) \rightarrow \mathrm{H}(1s)\text{-}\mathrm{H_2O}^{+(*)} + e'$] as functions of the energy of the incoming electron averaged over all scattering symmetries and multiplied by $R^6$. The results computed with the $R$-matrix approach are compared with those of the virtual photon approximation. The electron energy is given with respect to the initial ICEC state (see Table I). The cross sections obtained from the virtual photon approximation were multiplied by 2. This factor is explained by the different levels of theory employed to compute the photoionization cross sections (see [33–35]) entering in Eq. (1), compared to the electronic structure calculations used in the $R$-matrix approach. The *ab initio* ICEC cross section for the proton-neon dimer, shifted by −6.8 eV, is also shown for comparison. This cross section does not exhibit Fano profiles because the respective resonances lie much higher in energy (see main text).

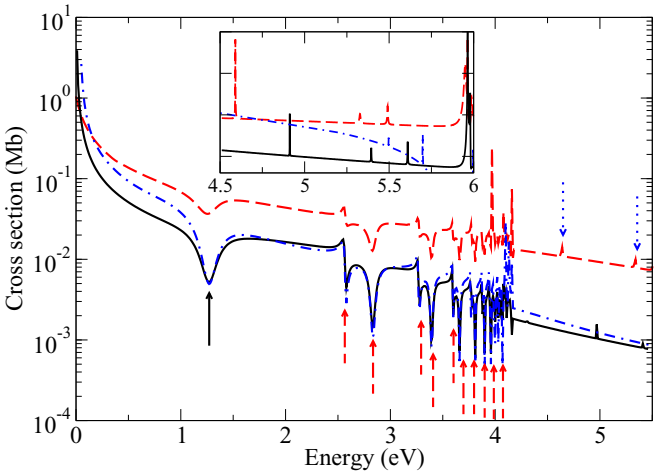


FIG. 3. ICEC cross sections for the $A_1$ scattering symmetry as functions of the incoming electron energy. The cross sections were obtained with the $R$-matrix method for different $R$ (same color code as in Fig. 2). In the inset, the cross sections for $R = 10$ Å were multiplied by 10 such that the profiles can be clearly seen. Additional CI calculations allowed us to assign the $(N + 1)$-electron states that interfere with the ICEC final states: the full black, red dashed, and blue dotted arrows indicate the interferences with $\mathrm{H}(1s)\text{-}\mathrm{H_2O}(^3A_1, 1b_2 \rightarrow 2b_2)$, $\mathrm{H}(1s)\text{-}\mathrm{H_2O}(^1A_1, 1b_2 \rightarrow b_2)$, and ion pair states, respectively (see main text). The electron energy is given with respect to the initial ICEC state (see Table I).

between H and $H_2O$, which are neglected in the asymptotic derivation (see [21,22] and [26]).

As shown in Fig. 2, the *ab initio* ICEC cross sections exhibit some structures that are superimposed to the smooth cross sections computed within the virtual photon approximation. As discussed below, these structures are Fano profiles coming from the interference between two pathways leading to the same final states: the direct ICEC pathway and that via metastable electronic states of the $(N + 1)$-electron system. For comparison, we computed the ICEC cross sections for the proton-neon dimer for an internuclear distance of 8 Å, which is isoelectronic to the proton-water one. We employed the cc-pVDZ basis set, and the CASSCF orbitals optimized for the two lowest singlet $A_1$ states were used. This model provides a similar description as the one used for the proton-water setup. The total cross sections are also shown in Fig. 2. Owing to the higher ionization potential of neon compared to water, ICEC opens only at electron energy above 6.8 eV in our calculations. To be graphically comparable with the results of the proton-water setup in Fig. 2, we have shifted the electron energy by −6.8 eV for this system. No Fano profiles are observed for the proton-neon dimer: the lowest H-Ne states lie higher in energy than those reachable for the incoming electron energies shown and, therefore, no interference is possible. This contrasts with the appearance of the Fano profiles observed in the *ab initio* ICEC cross sections of the proton-water setup.

The ICEC cross sections obtained with the $R$-matrix approach the scattering symmetry $A_1$ are shown in Fig. 3. As in the total cross sections, Fano profiles are clearly seen. We have performed additional CI calculations using MOLPRO and the same basis set and active space as those used for the target states in the $R$-matrix calculations. These additional calculations allow us to assign the character of the resonant states that interfere with the ICEC final states. The computations show that the Fano profile located at about 1.3 eV arises due to the interference with the state $\mathrm{H}(1s)\text{-}\mathrm{H_2O}(^3A_1, 1b_2 \rightarrow 2b_2)$. The next one in energy stems from the corresponding singlet excitation of water, i.e., from the interference with the $\mathrm{H}(1s)\text{-}\mathrm{H_2O}(^1A_1, 1b_2 \rightarrow 2b_2)$ resonant state. In Fig. 3, the higher Fano profiles up to about 4.2 eV [i.e., the $\mathrm{H}(1s)\text{-}\mathrm{H_2O}^+(^2B_2)$ ionization threshold] are related to the $\mathrm{H}(1s)\text{-}\mathrm{H_2O}(^1A_1, 1b_2 \rightarrow$ Rydberg) resonant states. It should be noted that the lowest Fano profile corresponds to a triplet excited state of water. The transition from the ground electronic state of water to such an excited state is spin forbidden, leading to a different shape of the Fano profile from that of the higher ones (see below).

The profiles below 4.2 eV correspond to resonant states where both species are neutral. The energy position of these states thus does not change significantly with $R$. In contrast, we see above the energy of 4.2 eV, in Fig. 3 and its inset, profiles whose position varies in inverse proportion to the proton-water distance, unambiguously indicating interference with ion pair resonant states (i.e., $\mathrm{H}^+\text{-}\mathrm{H_2O}^-$ and $\mathrm{H}^{-*}\text{-}\mathrm{H_2O}^+$). The CI calculations show that there are several ion pair resonant states of both kinds in the respective energy range, but a detailed assignment of the peaks to specific states is beyond

the present ability of the code. The $H^+$-$H_2O^-$ resonances can be populated by the incoming electron attaching to the water. Compared to isolated water, these resonances are stabilized by the presence of the proton. In contrast, the resonances of the type $H^{-*}$-$H_2O^+$ cannot be populated directly by attaching the electron to the proton: their population requires a long-range electron transfer from the water to the proton. On the other hand, for the resonances to contribute to the ICEC cross section, the latter type can directly emit an electron, while the decay of the former type of resonance is more intricate. Here, the resonance decays via a well-studied mechanism called electron transfer mediated decay (ETMD) [36–39]. In ETMD, the neighbor donates an electron and the excess energy is utilized to emit another electron from the neighbor. In our case, the water anion transfers an electron to the proton, thus neutralizing it, and the energy gained is utilized to turn the water into a water cation, giving rise to $H^+$-$H_2O^- \rightarrow H(1s)$ - $H_2O^+ + e'$ which is a final state of ICEC. It is remarkable that the signature of such long-range multielectron processes can be seen in the ICEC cross section, even at extremely large interspecies distances.

In order to gain further insights into the interferences between the quantum paths, we analyze the profiles below 4.2 eV seen in Fig. 3. In the vicinity of each profile, the cross sections should follow the general Fano form (see [1]),

$$\sigma \propto \frac{(\tilde{E}+q)^2}{1+\tilde{E}^2}. \tag{2}$$

In the above equation, $q$ is the asymmetry parameter and $\tilde{E}$ is called the reduced energy,

$$\tilde{E} = 2(\epsilon - E_i)/\Gamma_i, \tag{3}$$

where $E_i$ and $\Gamma_i$ are, respectively, the position and width of the resonant state. In Fano theory, the asymmetry parameter $q$ is a central quantity which is defined as a ratio of the transition probabilities to the resonant state and to the continuum. When the asymmetry parameter $|q|$ is of the order of 1, the transitions through the continuum and resonant state are of the same strength, resulting in the asymmetric Fano profile. In the limit where $|q|$ is very large, the transition to the continuum is very weak and the transition through the resonant state largely dominates. Conversely, in the case where $q = 0$, the cross section is described by a symmetrical dip around the position of the resonant state.

It is evident from the line shape around the profiles that the lowest one is characterized by an asymmetry parameter $|q|$ close to zero, while that for the higher ones is near unity. We have fitted the cross sections using Eq. (2) around these profiles and, indeed, found $q = 0.03$ for the lowest profile and between 0.6 and 1.0 for the higher ones. This shows that around the incoming electron energy of 1.3 eV, the ICEC process is mostly a direct process. It should be noted, however, that although there is almost no transition through the resonant state, the presence of the latter leads to a substantial decrease of the ICEC cross sections in the respective electron energy range. At higher electron energies, the paths through the resonant states play an equally important role as the direct one.

## IV. CONCLUSIONS

In this work, we have theoretically investigated the interatomic Coulombic electron capture process with the *ab initio* *R*-matrix method. ICEC is an efficient long-range energy transfer process relevant in various contexts where electron scattering drives the physics and chemistry of a system in an environment. In the example of a proton in the neighborhood of a water molecule, we have shown that the ICEC cross sections exhibit clear Fano profiles. The latter stem from the interferences between the ICEC final states and resonant states in which the incoming electron temporarily binds to the proton-water setup. Due to these interferences, the ICEC cross sections can be substantially enhanced or suppressed. Such phenomena are expected to be a common feature of ICEC and should thus be important in research fields where electron scattering in an environment takes place. Furthermore, collisions between electrons and molecules, especially water, have attracted considerable attention in the most recent decade owing to their crucial role in a great variety of processes. Our work demonstrates that the presence of a cation near the molecules substantially changes the scattering processes and their cross sections, opening new research directions.

## ACKNOWLEDGMENTS

This project has received funding from the LabEx MiChem part of the French state funds managed by the ANR within the "Investissements d'Avenir" program under Reference No. ANR-11-IDEX-0004-02. L.S.C. is thankful for support by the European 5448 Research Council (Advanced Investigator Grant No. 692657). J.D.G. acknowledges support from the -AMOR consortium (EPSRC Grant No. EP/R029342/1).

[1] U. Fano, Phys. Rev. **124**, 1866 (1961).
[2] U. Fano and J. W. Cooper, Phys. Rev. **137**, A1364 (1965).
[3] A. C. LaForge, D. Regina, G. Jabbari, K. Gokhberg, N. V. Kryzhevoi, S. R. Krishnan, M. Hess, P. O'Keeffe, A. Ciavardini, K. C. Prince, R. Richter, F. Stienkemeier, L. S. Cederbaum, T. Pfeifer, R. Moshammer, and M. Mudrich, Phys. Rev. A **93**, 050502(R) (2016).
[4] J. Feist, F. Capasso, C. Sirtori, K. W. West, and L. N. Pfeiffer, Nature (London) **390**, 589 (1997).
[5] H. Schmidt, K. L. Campman, A. C. Gossard, and A. Imamoglu, Appl. Phys. Lett. **70**, 3455 (1997).
[6] M. Allan, J. Phys. B **38**, 603 (2005).
[7] C. Winstead and V. McKoy, Phys. Rev. A **57**, 3589 (1998).
[8] S. Rotter, F. Libisch, J. Burgdörfer, U. Kuhl, and H. J. Stöckmann, Phys. Rev. E **69**, 046208 (2004).
[9] F. Cerdeira, T. A. Fjeldly, and M. Cardona, Phys. Rev. B **8**, 4734 (1973).
[10] R. Gupta, Q. Xiong, C. K. Adu, U. J. Kim, and P. C. Eklund, Nano Lett. **3**, 627 (2003).
[11] V. Madhavan, W. Chen, T. Jamneala, M. Crommie, and S. Wingreen, Science **280**, 567 (1998).

[12] O. Ujsaghy, J. Kroha, L. Szunyogh, and A. Zawadowski, Phys. Rev. Lett. **85**, 2557 (2000).
[13] H. G. Luo, T. Xiang, X. Q. Wang, Z. B. Su, and L. Yu, Phys. Rev. Lett. **92**, 256602 (2004).
[14] J. Göres, D. Goldhaber-Gordon, S. Heemeyer, M. A. Kastner, H. Shtrikman, D. Mahalu, and U. Meirav, Phys. Rev. B **62**, 2188 (2000).
[15] C.-M. Ryu and S. Y. Cho, Phys. Rev. B **58**, 3572 (1998).
[16] W. Hofstetter, J. König, and H. Schoeller, Phys. Rev. Lett. **87**, 156803 (2001).
[17] K. Kobayashi, H. Aikawa, S. Katsumoto, and Y. Iye, Phys. Rev. Lett. **88**, 256806 (2002).
[18] J. Kim, J.-R. Kim, J.-O. Lee, J. W. Park, H. M. So, N. Kim, K. Kang, K.-H. Yoo, and J.-J. Kim, Phys. Rev. Lett. **90**, 166403 (2003).
[19] W. Yi, L. Lu, H. Hu, Z. W. Pan, and S. S. Xie, Phys. Rev. Lett. **91**, 076801 (2003).
[20] B. Luk'yanchuk, N. I. Zheludev, S. A. Maier, N. J. Halas, P. Nordlander, H. Giessen, and C. T. Chong, Nat. Mater. **9**, 707 (2010).
[21] K. Gokhberg and L. S. Cederbaum, J. Phys. B **42**, 231001 (2009).
[22] K. Gokhberg and L. S. Cederbaum, Phys. Rev. A **82**, 052707 (2010).
[23] A. Bande, K. Gokhberg, and L. S. Cederbaum, J. Chem. Phys. **135**, 144112 (2011).
[24] F. M. Pont, A. Bande, and L. S. Cederbaum, Phys. Rev. B **88**, 241304(R) (2013).
[25] A. Molle, E. R. Berikaa, F. M. Pont, and A. Bande, J. Chem. Phys. **150**, 224105 (2019).
[26] N. Sisourat, T. Miteva, J. D. Gorfinkiel, K. Gokhberg, and L. S. Cederbaum, Phys. Rev. A **98**, 020701(R) (2018).
[27] J. Tennyson, Phys. Rep. **491**, 29 (2010).
[28] Z. Mašín, J. Benda, J. D. Gorfinkiel, A. G. Harvey, and J. Tennyson, Comput. Phys. Commun. **249**, 107092 (2020).
[29] H.-J. Werner, P. J. Knowles, G. Knizia, F. R. Manby, and M. Schütz, WIREs Comput. Mol. Sci. **2**, 242 (2012).
[30] H.-J. Werner, P. J. Knowles, G. Knizia, F. R. Manby, M. Schütz, P. Celani, W. Györffy, D. Kats, T. Korona, R. Lindh, A. Mitrushenkov, G. Rauhut, K. R. Shamasundar, T. B. Adler, R. D. Amos, A. Bernhardsson, A. Berning, D. L. Cooper, M. J. O. Deegan, A. J. Dobbyn, F. Eckert, E. Goll, C. Hampel, A. Hesselmann, G. Hetzer, T. Hrenar, G. Jansen, C. Köppl, Y. Liu, A. W. Lloyd, R. A. Mata, A. J. May, S. J. McNicholas, W. Meyer, M. E. Mura, A. Nicklass, D. P. O'Neill, P. Palmieri, D. Peng, K. Pflüger, R. Pitzer, M. Reiher, T. Shiozaki, H. Stoll, A. J. Stone, R. Tarroni, T. Thorsteinsson, and M. Wang, Computer software "MOLPRO, version 2015.1, A package of *ab initio* programs" (2015), https://www.molpro.net/
[31] A. W. Potts and W. C. Price, Proc. Roy. Soc. London A **326**, 181 (1972).
[32] M. Rubio, L. Serrano-Andrés, and M. Merchán, J. Chem. Phys. **128**, 104305 (2008).
[33] W. Cunto, C. Mendoza, F. Ochsenbein, and C. J. Zeippen, Bulletin d'Information du Centre de Donnees Stellaires **42**, 39 (1993).
[34] The Leiden database for photodissociation and photoionization of astrophysically relevant molecules, https://home.strw.leidenuniv.nl/~ewine/photo/cross_sections.html.
[35] A. N. Heays, A. D. Bosman, and E. F. van Dishoeck, A&A **602**, A105 (2017).
[36] J. Zobeley, R. Santra, and L. S. Cederbaum, J. Chem. Phys. **115**, 5076 (2001).
[37] K. Sakai, S. Stoychev, T. Ouchi, I. Higuchi, M. Schöffler, T. Mazza, H. Fukuzawa, K. Nagaya, M. Yao, Y. Tamenori, A. I. Kuleff, N. Saito, and K. Ueda, Phys. Rev. Lett. **106**, 033401 (2011).
[38] M. Förstel, M. Mucke, T. Arion, A. M. Bradshaw, and U. Hergenhahn, Phys. Rev. Lett. **106**, 033402 (2011).
[39] D. You, H. Fukuzawa, Y. Sakakibara, T. Takanashi, Y. Ito, G. G. Maliyar, K. Motomura, K. Nagaya, T. Nishiyama, K. Asa, Y. Sato, N. Saito, M. Oura, M. Schöffler, G. Kastirke, U. Hergenhahn, V. Stumpf, K. Gokhberg, A. I. Kuleff, L. S. Cederbaum, and K. Ueda, Nat. Commun. **8**, 14277 (2017).